The length of lipids bound to human CD1d molecules modulates the affinity of NKT cell TCR and the threshold of NKT cell activation

Corinna McCarthy,[1] Dawn Shepherd,[1] Sebastian Fleire,[4] Victoria S. Stronge,[1] Michael Koch,[2] Petr A. Illarionov,[5] Giovanna Bossi,[3] Mariolina Salio,[1] Galit Denkberg,[6] Faye Reddington,[5] Andrea Tarlton,[1] B. Gopal Reddy,[7] Richard R. Schmidt,[7] Yoram Reiter,[6] Gillian M. Griffiths,[3] P. Anton van der Merwe,[3] Gurdyal S. Besra,[5] E. Yvonne Jones,[2] Facundo D. Batista,[4] and Vincenzo Cerundolo[1]

[1]Tumour Immunology Unit, Weatherall Institute of Molecular Medicine, John Radcliffe Hospital, [2]Cancer Research UK Receptor Structure Research Group, Division of Structural Biology, Wellcome Trust Centre for Human Genetics, and [3]Sir William Dunn School of Pathology, University of Oxford, Oxford OX3 9DS, UK
[4]Lymphocyte Interaction Laboratory, London Research Institute, Cancer Research UK, London WC2A 3PX, UK
[5]School of Biosciences, University of Birmingham, Edgbaston, Birmingham B15 2TT, UK
[6]Faculty of Biology, Technion-Israel Institute of Technology, Haifa 32000, Israel
[7]Fachbereich Chemie, Universitaet Konstanz, D-78457 Konstanz, Germany

CD1d-restricted lymphocytes recognize a broad lipid range. However, how CD1d-restricted lymphocytes translate T cell receptor (TCR) recognition of lipids with similar group heads into distinct biological responses remains unclear. Using a soluble invariant NKT (iNKT) TCR and a newly engineered antibody specific for α-galactosylceramide (α-GalCer)–human CD1d (hCD1d) complexes, we measured the affinity of binding of iNKT TCR to hCD1d molecules loaded with a panel of α-GalCer analogues and assessed the rate of dissociation of α-GalCer and α-GalCer analogues from hCD1d molecules. We extended this analysis by studying iNKT cell synapse formation and iNKT cell activation by the same panel of α-GalCer analogues. Our results indicate the unique role of the lipid chain occupying the hCD1d F′ channel in modulating TCR binding affinity to hCD1d–lipid complexes, the formation of stable immunological synapse, and cell activation. These data are consistent with previously described conformational changes between empty and loaded hCD1d molecules (Koch, M., V.S. Stronge, D. Shepherd, S.D. Gadola, B. Mathew, G. Ritter, A.R. Fersht, G.S. Besra, R.R. Schmidt, E.Y. Jones, and V. Cerundolo. 2005. *Nat. Immunol* 6:819–826), suggesting that incomplete occupation of the hCD1d F′ channel results in conformational differences at the TCR recognition surface. This indirect effect provides a general mechanism by which lipid-specific lymphocytes are capable of recognizing both the group head and the length of lipid antigens, ensuring greater specificity of antigen recognition.

CORRESPONDENCE
Vincenzo Cerundolo:
vincenzo.cerundolo@imm.ox.ac.uk

Abbreviations used: α-GalCer, α-galactosylceramide; cSMAC, central SMAC; GPI, glycosylphosphatidylinositol; GSL, glycosphingolipid; hCD1d, human CD1d; iNKT, invariant NKT; IRM, interference reflection microscopy; SMAC, supramolecular activation cluster; SPR, surface plasmon resonance.

CD1d-restricted lymphocytes contribute to antimicrobial host responses in bacterial, parasitic, viral, and fungal infections and to the natural antitumor response (1). Broad specificity of CD1d-restricted T cells is the result of the ability of CD1d molecules to bind a range of lipids (1, 2). More recently, it has been shown that mouse and human NKT cells can also recognize bacteria-derived diacylglycerol (3), thus demonstrating the ability of NKT cells to recognize glycolipids as well as glycosphingolipids (GSLs). The ability of CD1d-restricted lymphocytes to recognize a broad range of self and nonself lipids highlights the importance of understanding the parameters controlling both their activation in vivo and the mechanisms by which the cross-reactivity of lipid-specific CD1d-restricted T cells is minimized.

The antigen-binding site of mouse and human CD1d (hCD1d) molecules is composed of two channels: A′ and F′ channels in mouse

C. McCarthy, D. Shepherd, and S. Fleire contributed equally to this paper.
The online version of this article contains supplemental material.

CD1d, which connect directly to the surface. For consistency with the mouse CD1d literature, the phytosphingosine chain–binding channel in hCD1d, which is referred to as the C′ channel by Koch et al. (4), is here referred to as the F′ channel (5–9). Although the A′ channel can accommodate an alkyl chain up to 26 carbon atoms long, the F′ channel can accommodate an alkyl chain up to 18 carbon atoms long. hCD1d molecules in which the A′ and F′ channels are not filled (i.e., that are in the nonlipid-bound state) have a different conformation than hCD1d molecules bound to α-galactosylceramide (α-GalCer; reference 4). Whereas the entrance of the cavity is wider in the empty conformation, the volumes of the A′ and F′ channels are reduced, mostly as a result of the conformational shifts in the side chains of several tryptophan residues. The recently solved crystal structures of CD1d–α-GalCer–specific TCR and docking models (10, 11) are consistent with the TCR binding footprint encompassing the polar head of the lipid ligand and portions of the CD1d α1 and α2 helices but do not support direct interactions between the TCR and the lipid alkyl chains.

The knowledge derived from the structure of CD1d–α-GalCer–specific TCRs and from the structure of empty and α-GalCer–loaded hCD1d molecules prompted us to carry out a series of kinetic and functional experiments to assess the role of the length of each alkyl chain in controlling the rate of dissociation of lipids bound to hCD1d molecules and the affinity of binding of lipid-specific TCR. An important parameter to consider in evaluating the biological effects of NKT agonists is the affinity of TCR binding to the glycolipid–CD1d complex and the stability of glycolipid ligands bound to CD1d molecules. It has been shown that the compound OCH, which is an analogue of α-GalCer with a truncated sphingosine chain, binds less stably to CD1d compared with α-GalCer, resulting in a less sustained TCR stimulation and secretion of higher amounts of IL-4 than IFN-γ by NKT cells (12, 13). To further probe these questions and to address the role of lipid length and saturation in influencing CD1d-restricted T cell responses, we engineered a soluble TCR from an invariant NKT (iNKT) cell clone and an antibody specific for the hCD1d–α-GalCer complex. Using these two reagents, we performed combined kinetic and functional studies to compare the affinity of TCR binding to hCD1d molecules loaded with either α-GalCer or analogues of α-GalCer with truncated acyl and phytosphingosine chains. In this set of analogues, we included OCH9, which has a shorter phytosphingosine chain than α-GalCer and differs from the previously described OCH by the addition of two methylene groups on the acyl chain (12, 13). We also assessed whether

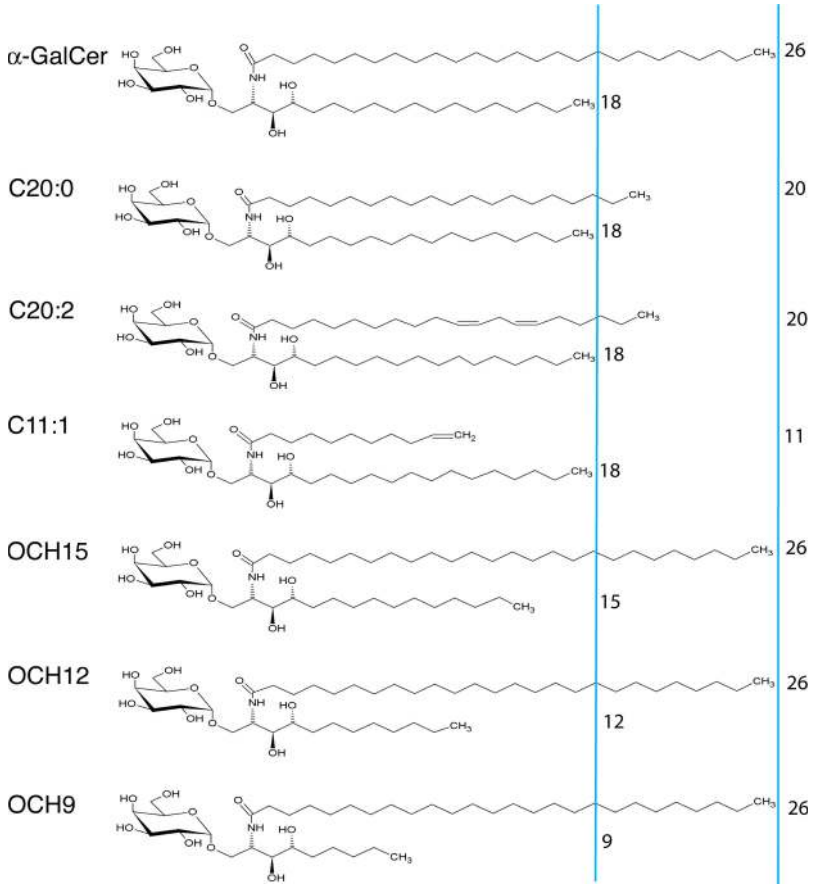

Figure 1. Glycolipids used in this study. The lengths of acyl and phytosphingosine chains are indicated.

the presence of unsaturated double bonds in the acyl chains could affect the rate of lipid dissociation from hCD1d molecules and the affinity of TCR binding to hCD1d–glycolipid complexes. We extended these results by assessing both the immunological synapse and lymphokine profile of human iNKT cells stimulated with the same panel of glycolipids.

The results of these experiments demonstrated that although the length of both phytosphingosine and acyl chains controls the stability of lipids bound to hCD1d molecules, the length of the phytosphingosine chain, but not the length and saturation of the acyl chain, controls the affinity of TCR binding to hCD1d–glycolipid complexes and iNKT cell activation. We propose a model involving the propagation of conformational changes from within the binding groove to the surface that is consistent with the observed effects on TCR binding. Because natural lipids have a broad range of acyl chain lengths (14), our results are of general importance, as they suggest a mechanism by which lipid-specific lymphocytes can distinguish individual lipids based on both the headgroup and the length of the lipid chain occupying the CD1d F′ channel.

RESULTS

The length of the phytosphingosine chain modulates iNKT TCR binding affinity to the hCD1d–GSL complex

We refolded hCD1d with a range of α-GalCer analogues with truncated acyl or phytosphingosine chains (Fig. 1). We then analyzed the rate of dissociation of each GSL from hCD1d molecules (Fig. 2 A) and the kinetics of iNKT TCR binding to each hCD1d–GSL monomer (Fig. 2 B). To measure the dissociation of each GSL from hCD1d molecules, we generated by phage display library a Fab antibody specific for hCD1d molecules loaded with α-GalCer (hereafter referred to as Fab 9B; unpublished data). Initial surface plasmon resonance (SPR) measurements and FACS staining of lipid-pulsed C1R-hCD1d cells demonstrated that Fab 9B specifically recognized hCD1d molecules loaded with the GSL shown in Fig. 1, whereas it failed to stain either unpulsed C1R-hCD1d cells or C1R-hCD1d cells pulsed with β-GalCer (unpublished data). Using Fab 9B, we measured the GSL dissociation from soluble hCD1d molecules over time using SPR (Fig. 2 A). We observed that shortening either the acyl chain or the phytosphingosine chain increased the rate of lipid dissociation from hCD1d molecules (Fig. 2 A). Interestingly, the rate of dissociation of compound C20:0 is 2.15-fold faster than that of compound C20:2 (half-life of 170 min and 367 min, respectively, at 25°C), demonstrating that unsaturation of bonds at carbons 11 and 14 of the acyl chain favors the formation of more stable hCD1d–GSL complexes.

We then assessed whether the length of the acyl and phytosphingosine chains could affect the affinity of iNKT TCR binding to the hCD1d–GSL complex. We refolded Vα24 and Vβ11 chains of iNKT TCR as previously described (10) and used the purified and refolded iNKT TCR in SPR studies against immobilized biotinylated hCD1d–GSL monomers. We demonstrated that the affinity of iNKT TCR for hCD1d–α-GalCer was substantially higher than that of hCD1d–OCH9 (Kd of 1.6 μM compared with 122 μM; Fig. 2 B).

To further understand the contribution of phytosphingosine chain length to the iNKT cell TCR affinity, we compared the affinity of iNKT TCR binding to hCD1d–OCH9 complexes with that of hCD1d molecules loaded either with OCH12 or OCH15 (Fig. 2 B, bottom). These experiments demonstrated that increasing the phytosphingosine chain length from 9 to 15 carbons increased the iNKT TCR binding affinity, suggesting that optimal iNKT TCR binding requires the lipid chain occupying the hCD1d F′ channel to range from 15 to 18 carbons. In contrast, the length and saturation of the fatty acid chain did not substantially alter the iNKT TCR binding affinity (Fig. 2 B, middle). Analysis of the binding of the anti-β2M antibody (BBM.1) confirmed that equivalent amounts of correctly refolded hCD1d–ligand complexes were immobilized to each sensor surface (unpublished data). As a further control, we showed that differences in the iNKT TCR binding affinity were not the result of differences in loading of hCD1d monomers with α-GalCer, OCH12, and OCH9 (Fig. S1, available at http://www.jem.org/cgi/content/full/jem.20062342/DC1). The rate constants (k_{on} and k_{off}) of iNKT TCR binding were measured directly for all hCD1d–GSL complexes with the exception of hCD1d–OCH9, in which the exceptionally fast k_{off} made

Table I. Affinity and kinetics measurements

hCD1d–GSL complex	Kd	k_{off}	k_{on}	k_{on}
	μM	*S^{-1}*	*$M^{-1}S^{-1}$*	*$M^{-1}S^{-1}$*
α-GalCer	1.29 ± 0.08[a]	0.39 ± 0.01[a]	$3.31 \times 10^5 \pm 2.5 \times 10^4$[a]	$3.10 \times 10^5 \pm 4.0 \times 10^4$[a]
C20:0	2.73 ± 0.69[a]	0.58 ± 0.07	$2.38 \times 10^5 \pm 4.6 \times 10^4$	$2.13 \times 10^5 \pm 1.9 \times 10^4$
C20:2	1.83 ± 0.13[a]	0.46 ± 0.06	$2.46 \times 10^5 \pm 2.3 \times 10^4$	$2.49 \times 10^5 \pm 1.1 \times 10^4$
C11:1	3.40 ± 0.39[a]	0.59 ± 0.04	$1.65 \times 10^5 \pm 3.5 \times 10^4$	$1.75 \times 10^5 \pm 2.6 \times 10^4$
OCH15	2.50 ± 0.36[a]	0.47 ± 0.06	$2.04 \times 10^5 \pm 1.6 \times 10^4$	$1.92 \times 10^5 \pm 2.5 \times 10^4$
OCH12	23.3 ± 1.41[a]	1.00 ± 0.12	$3.7 \times 10^4 \pm 5 \times 10^3$	$4.3 \times 10^4 \pm 6 \times 10^3$
OCH9	123 ± 9.08[a]	2.67 ± 0.12[a]	ND	$2.3 \times 10^4 \pm 1 \times 10^3$

All values are the mean of two experiments except where otherwise noted. The k_{on} values were experimentally determined by SPR except those in the last column, which were calculated from the experimentally determined k_{off} and Kd values.
[a]Mean of three or more experiments.

direct determination of the k_{on} difficult. Nevertheless, it was possible to calculate k_{on} for iNKT TCR binding to hCD1d–OCH9 from the Kd and k_{off} (Table I). Comparison of the binding kinetics of iNKT TCR to the hCD1d–GSL monomers demonstrated that the decrease in affinity observed with shortening the phytosphingosine chain was as much the result of decreases in the k_{on} as increases in the k_{off} (Fig. 2 B and Table I). Agreement was observed between the affinities calculated from the kinetic constants and the affinities determined by equilibrium binding (Table I and unpublished data).

To ensure that differences in the affinity of iNKT TCR binding to hCD1d–GSL complexes were physiologically

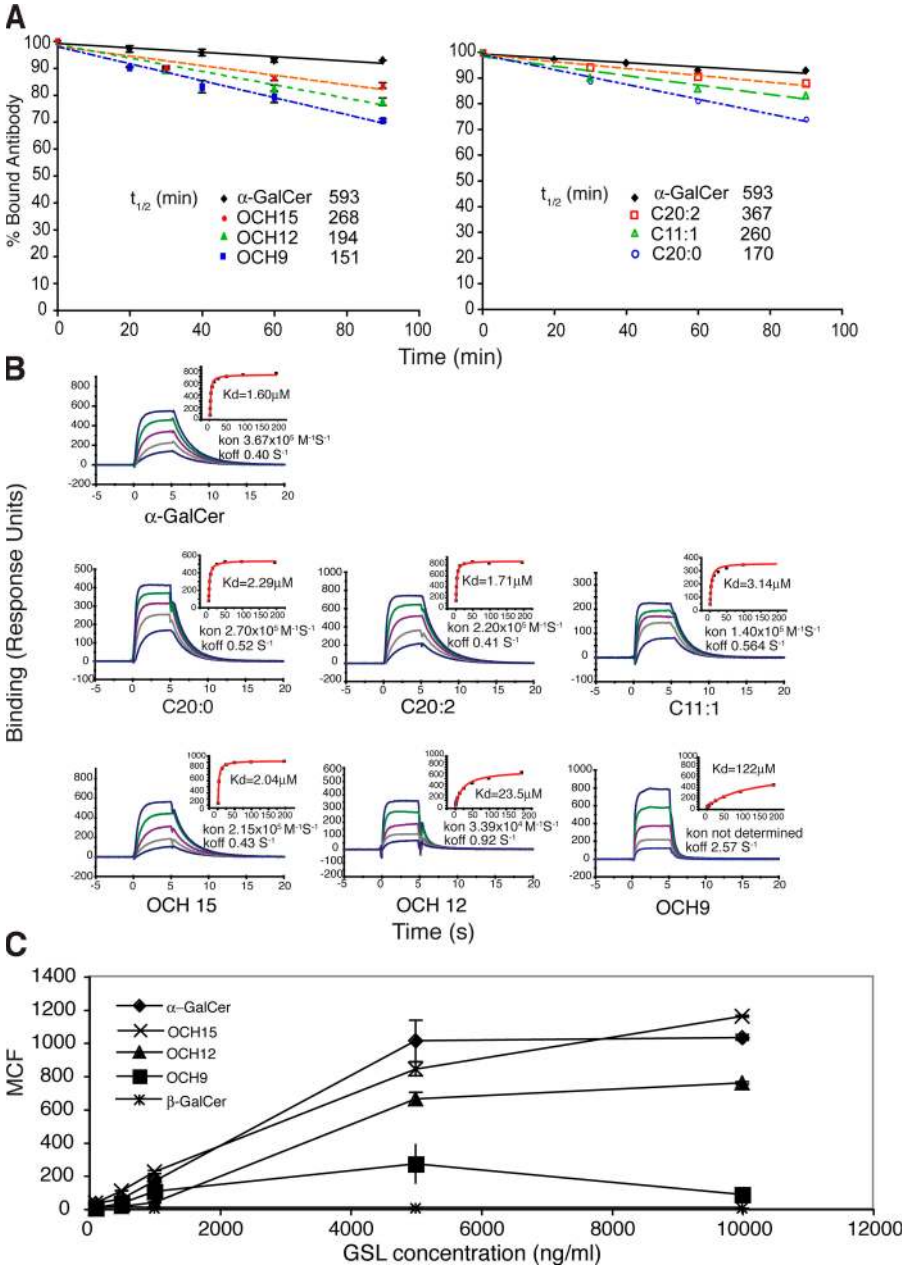

Figure 2. Affinity and kinetics of GSL binding to hCD1d and iNKT TCR binding to the hCD1d–GSL complex. (A) Dissociation of GSL from hCD1d. The indicated hCD1d–GSL complex was loaded onto a sensor surface at t = 0, and the amount of hCD1d remaining at the indicated time point was measured using Fab 9B. (B) Affinity and kinetics of iNKT TCR binding to hCD1d complexed with α-GalCer (top), C20:0, C20:2, and C11:1 (middle), and OCH15, OCH12, and OCH9 (bottom). Increasing concentrations from 0.4 to 194 μM (twofold dilution) of iNKT TCR were injected for 5 s over the indicated hCD1d–GSL complexes. The binding responses of five concentrations are shown superimposed. The insets show binding response at equilibrium. A representative experiment is shown. (C) C1R-hCD1d cells were pulsed with the GSLs shown and were stained with the biotinylated tetramerized iNKT TCR. Mean channel fluorescence (MCF) as determined by FACS is shown to vary with the TCR affinity as measured by SPR studies. A representative experiment out of three is shown.

relevant, we used biotinylated iNKT TCR to stain C1R-hCD1d cells pulsed with a panel of GSL (Fig. 2 C). The results of these experiments confirmed that C1R-hCD1d cells pulsed with α-GalCer and OCH15 were stained more efficiently than C1R-hCD1d pulsed with either OCH12 or OCH9 (Fig. 2 C). As a control, GSL-pulsed C1R-hCD1d cells were stained with the Fab 9B antibody to ensure a similar loading of hCD1d molecules by the panel of GSL at a concentration of 10 μg/ml (Fig. S2, available at http://www.jem.org/cgi/content/full/jem.20062342/DC1).

iNKT cells form classical immunological synapses in response to hCD1d–GSL complexes

To extend our findings on the molecular aspects of the iNKT cell immunological synapse and to investigate the possibility that differences in iNKT TCR affinity for the various hCD1d–GSL

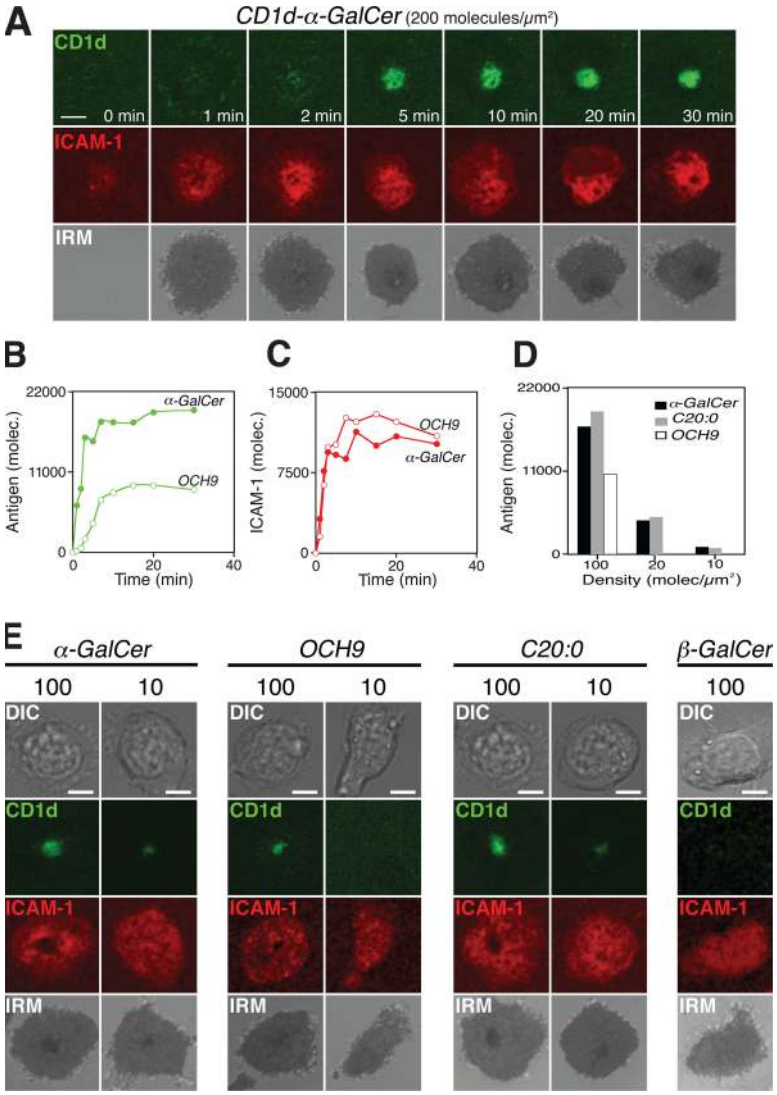

Figure 3. Kinetics and threshold of human iNKT cell synapse formation. (A) Time lapse of the interaction of an iNKT cell with an artificial lipid bilayer loaded with hCD1d–α-GalCer antigen at a density of 200 molecules/μm² (green) and ICAM-1 at a density of 80 molecules/μm² (red) as visualized by confocal microscopy. Contacts of the iNKT cell with the bilayer were visualized by IRM (grayscale, bottom). (B and C) The amount of hCD1d-ligand (B) and ICAM-1 (C) aggregated were quantified as a function of time for hCD1d–α-GalCer (closed circles) and hCD1d–OCH9 (open circles). All of the data is representative of at least 20 cells in three independent experiments. Loading of lipid bilayers with either hCD1d–α-GalCer or hCD1d–OCH9 monomers was normalized using Fab 9B, confirming a similar proportion of hCD1d monomers containing α-GalCer and OCH9 within the duration of each experiment. (D) The amount of antigen aggregated was quantified for the different ligands and densities as a function of time. ICAM-1 accumulation levels were equivalent in all of the cases (not depicted). (E) Synapse formation for the indicated ligands (α-GalCer, OCH9, C20:0, and β-GalCer) displayed at varying densities (top number in molecules/μm²) in the presence of ICAM-1 (density = 80 molecules/μm²) as visualized by confocal microscopy. A representative single cell after 30 min of interaction with the bilayer is shown in each column. Bars, 5 μm.

complexes may have an effect on the kinetics and/or pattern of hCD1d accumulation during synapse formation, we quantified the segregation and accumulation of hCD1d molecules and ICAM-1 in real time.

To this end, iNKT cells, from which the TCR for the kinetic studies was cloned, were settled onto bilayers containing AlexaFluor542-conjugated glycosyl-phosphatidylinositol (GPI)–linked ICAM-1 and biotinylated hCD1d monomers loaded with either α-GalCer or OCH9, which showed the greatest disparity in iNKT TCR affinity. We then followed the pattern of ICAM-1 (Fig. 3 A, red) and hCD1d (Fig. 3 A, green) distribution over time by confocal microscopy and correlated it with iNKT cell contact with the membrane as assessed by interference reflection microscopy (IRM), which allows the visualization of close membrane apposition as dark areas (Fig. 3 A).

We demonstrated that both hCD1d–OCH9 and hCD1d–α-GalCer monomers stimulated the formation of a classic immunological synapse, as characterized by the cessation of migration (Fig. 3 A and Video 1, available at http://www.jem.org/cgi/content/full/jem.20062342/DC1), the formation of a classic central supramolecular activation cluster (SMAC [cSMAC]), and aggregation of ICAM-1 to form a peripheral SMAC. This central zone of interaction was bordered by a ring of close apposition of the T cell membrane and planar bilayer (darkest area of IRM image). In the absence of ICAM-1 in the lipid bilayer, no clustering of hCD1d–α-GalCer molecules was observed (unpublished data). Quantification of the amount of hCD1d–α-GalCer–loaded molecules (Fig. 3 B) and ICAM-1 (Fig. 3 C) showed that a maximal clustering of both molecules was reached within 5 min and a plateau after 10 min. In contrast, quantification of the amounts of hCD1d–OCH9-loaded molecules (Fig. 3 B) showed slower kinetics and reduced maximal clustering of hCD1d–OCH9 monomers as compared with hCD1d–α-GalCer. Interestingly, consistent with the evidence that LFA-1 delivers a signal distinct from that of the TCR, accumulation of ICAM-1 to the peripheral SMAC was comparable between hCD1d–α-GalCer– and hCD1d–OCH9-stimulated synapses (Fig. 3 C). We also demonstrated that although hCD1d monomers loaded with β-GalCer did not induce any hCD1d clustering, some gathering of ICAM-1 was observed (Fig. 3 E). These results are consistent with previously published data analyzing the formation of the immunological synapse in T cells (15) and indicate that the affinity of the iNKT cells for hCD1d–GSL complexes may play an important role in determining ligand recognition.

To determine whether this difference in affinity translates into differential thresholds of hCD1d–GSL recognition, we compared the interaction of iNKT cells with lipid bilayers loaded with constant ICAM-1 concentration but decreasing densities of either hCD1d–α-GalCer or hCD1d–OCH9 monomers (Fig. 3, D and E). These results showed that a minimum density of 10 molecules/μm^2 was sufficient to trigger hCD1d–α-GalCer and hCD1d-C20:0 accumulation and immunological synapse formation (Fig. 3, D and E). In contrast, at this same density of hCD1d–OCH9, iNKT cells failed to aggregate antigen or show any sign of synapse formation. Indeed, a 10-fold increase in the density of hCD1d–OCH9 was required to observe similar frequencies of synapse formation. Because hCD1d–α-GalCer and hCD1d-C20:0 have a similar affinity of binding to iNKT

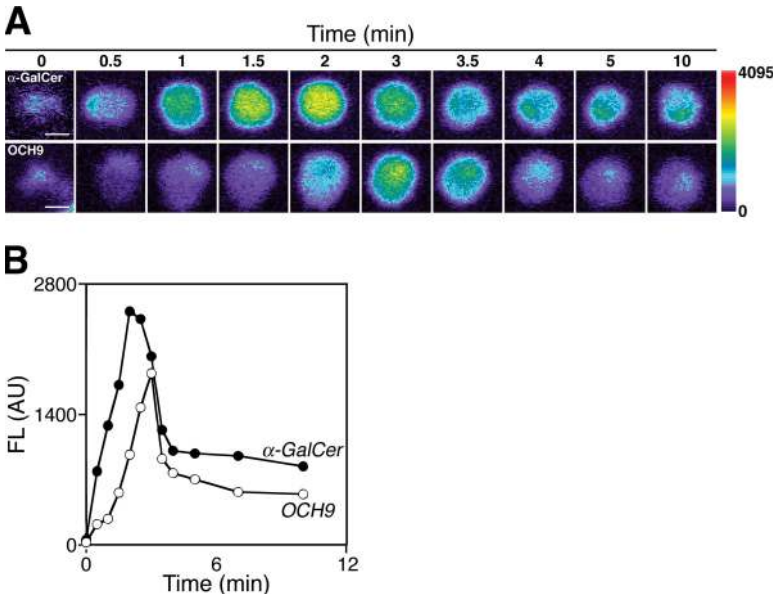

Figure 4. Calcium influx in response to the CD1d–ligands. (A) Kinetics of calcium influx of iNKT cells in contact with bilayers loaded with hCD1d–α-GalCer (top) or hCD1d–OCH9 (bottom) at a density of 200 molecules/μm^2 in the presence of ICAM-1 (density = 80 molecules/μm^2) as visualized by confocal microscopy. Fluorescence is shown in a pseudocolor scale. (B) The amount of intracellular calcium influx in fluorescence units (arbitrary units [AU]) for α-GalCer (closed circles) and OCH9 (open circles) quantified over a period of 10 min. Bars, 5 μm.

TCR (Fig. 2 B) and OCH9 and C20:0 have a similar rate of dissociation from hCD1d molecules (Fig. 2 A), these results demonstrate that the affinity of iNKT TCR determines the capacity of iNKT cells to cluster hCD1d–lipid complexes, and this may play a role in defining the threshold of iNKT cell activation.

Strength of iNKT cell stimulation is determined by the dynamics of synapse formation

To establish whether the differential accumulation of hCD1d–GSL complexes to the synapses correlated with the strength of the subsequent iNKT cell activation, we monitored the changes in intracellular calcium levels of iNKT cells stimulated with planar bilayers loaded with either hCD1d–α-GalCer or hCD1d–OCH9. At the same densities, hCD1d–α-GalCer–stimulated synapses resulted in a greater and more rapid fluxing of calcium into the iNKT cells compared with hCD1d–OCH9-stimulated synapses (Fig. 4, A and B). These results further support the concept that the length of the phytosphingosine chain of the lipid antigen is important in determining the threshold of iNKT cell activation.

To further assess the functional consequences of the differences in CD1d–GSL and TCR binding affinities, we analyzed the efficiency of polarization of iNKT cell lytic granules on the stimulation of iNKT cells with C1R- hCD1d target cells pulsed with either α-GalCer or OCH9, which are the strongest and weakest iNKT cell agonists, respectively. Titration of the lipid concentrations for both α-GalCer and OCH9

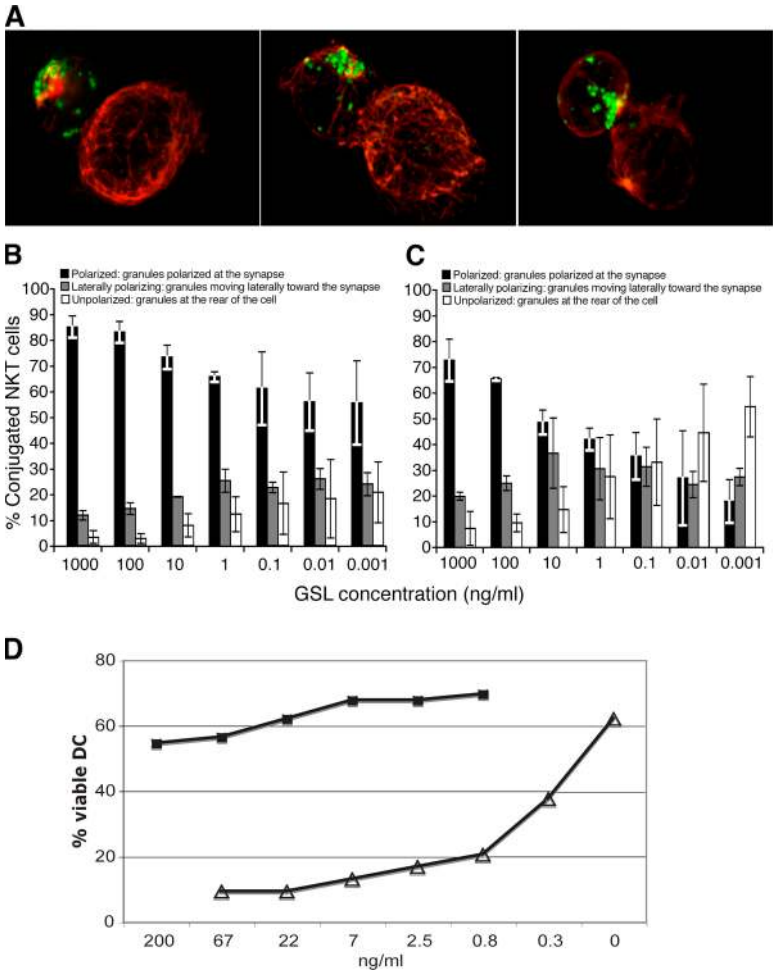

Figure 5. α-GalCer is efficient in inducing the polarization of iNKT cell granules at the immunological synapse. (A) The confocal images show iNKT cells conjugated with C1R-hCD1d cells pulsed with 1 μM α-GalCer. Lytic granules are stained with anti–cathepsin D (green) and both target and effector cells stained with antitubulin (red). Upon target cell recognition, lytic granules move from the rear of the cell (left), around the nucleus (middle), and polarize at the immunological synapse (right). (B and C) Quantitative analysis of granule polarization in iNKT cells recognizing C1R-hCD1d cells pulsed with α-GalCer (B) or OCH9 lipids (C). Cell conjugates with granules at the rear (white bars), granules moving laterally toward the synapse (gray bars), and granules at the synapse (black bars) were counted using a fluorescence microscope. (D) iNKT-dependent lysis of DCs pulsed with either α-GalCer or OCH9. Human monocyte-derived DCs were incubated with a human iNKT line at a ratio of 1:1 in the presence of different concentrations of α-GalCer (open triangles) or OCH9 (filled squares). After 24 h, DC viability was evaluated by FACS analysis gating on propidium iodide–negative cells. Error bars represent SD.

revealed that the number of polarized iNKT cells conjugated to targets was greatly reduced at lower concentrations of OCH9 when compared with α-GalCer (Fig. 5, B and C). When C1R-hCD1d cells were pulsed with OCH9, polarization was poor (i.e., 10 ng/ml OCH was required to see 50% of iNKT cell conjugates with tightly polarized granules at the synapse). In contrast, 0.001 ng/ml α-GalCer was sufficient to see 60% of iNKT cell conjugates with tightly polarized granules at the synapse. Because the affinity of Fab 9B for α-GalCer–CD1d and OCH9–CD1d monomers is very similar (Kd of 408 nM and 595 nM, respectively; unpublished data), FACS staining of C1R-hCD1d cells pulsed with 1 μM α-GalCer and OCH9 with Fab 9B confirmed that within the time frame of the experiment shown in Fig. 5, the amount of α-GalCer and OCH9 presented by C1R-hCD1d cells was comparable (not depicted). Consistent with the observed slower and less efficient polarization of cytotoxic granules of iNKT cells activated by OCH9, we demonstrated that human DCs pulsed with OCH9 were killed less efficiently by iNKT cells than human DCs pulsed with α-GalCer (Fig. 5 D).

iNKT cell TCR affinity for hCD1d–lipid complexes modulates iNKT cell activation

The density of clustered hCD1d–α-GalCer and the proportion of cells forming immunological synapses with α-GalCer as compared with OCH9 correlated with the in vitro activation of human iNKT cells as defined by IL-4 and IFN-γ secretion (Fig. 6 A). Furthermore, unlike results obtained with mouse iNKT cells (13, 16), the cytokine profile of human iNKT cells stimulated by OCH9 and OCH12 was not biased toward a Th2 response; rather, less IL-4 and IFN-γ were secreted (Fig. 6 A). Comparable cytokine profiles were obtained using iNKT cells stimulated with α-GalCer and with compounds with truncated acyl chains and OCH15. Thus, the pattern of cytokine production and target cell lysis by iNKT cells in response to lipid-pulsed target cells was consistent with the differential activation of iNKT cells.

Finally, we demonstrated the ability of both α-GalCer and OCH9 to stimulate the expansion of iNKT cells from peripheral blood lymphocytes from healthy donors (Fig. 6 B). Although α-GalCer was capable of sustaining iNKT cell proliferation at concentrations $< 10^{-11}$ M, OCH9 failed to induce iNKT cell proliferation at concentrations $<10^{-10}$ M, and, at all concentrations, α-GalCer stimulated greater numbers of iNKT cells.

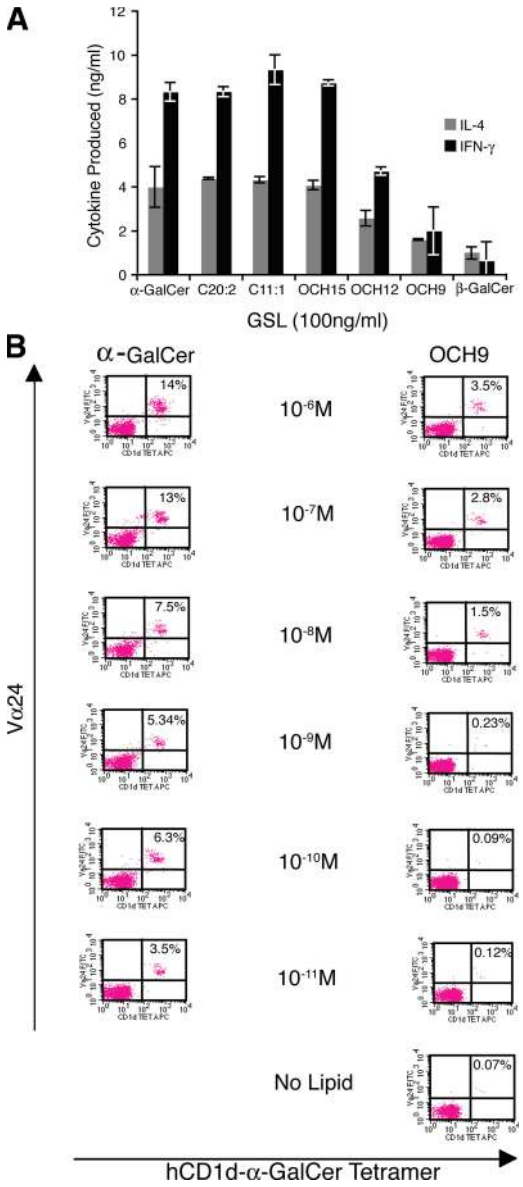

Figure 6. iNKT cell expansion and activation in vitro is modulated by the length of GSL sphyngosine chain. (A) CIR-hCD1d cells were pulsed with shown GSL and used to stimulate human iNKT cells. Supernatant was assayed for IL-4 (gray bars) or IFN-γ (black bars) by ELISA. SD from the mean (error bars) of two duplicate assays is shown. (B) iNKT cell frequency ($V\alpha24^+$hCD1d-tetramer$^+$ cells as the percentage of gated cells) on day 21 after stimulation of PBLs with mature autologous DCs pulsed with either α-GalCer or OCH9 at varying concentrations. Experiments were performed three times using three different healthy donors. The results of a representative experiment are shown.

DISCUSSION

Our results provide important insights into the mechanisms controlling lipid-specific T cell responses by demonstrating that modifications of the lipid chain buried in the F′ channel of hCD1d molecules can modulate the TCR affinity, formation of stable synapses, and, ultimately, lymphocyte activation. Previous studies have established that modifications of the alkyl chains may alter the activation of lipid-specific T cells (3, 13, 17–21). However, a combined kinetic and functional analysis has not been previously performed.

Because α-GalCer has the maximum lipid chain lengths that are able to fit into the antigen-binding groove of hCD1d and there are conformational differences between lipid-bound and nonlipid-bound CD1d molecules (4), we reasoned that binding of hCD1d molecules with analogues of α-GalCer containing shorter lipid chains may result in the partial collapse of unfilled portions of the A′ and F′ channels, resulting

in surface-exposed structural changes. This reasoning led us to study whether the binding affinity of soluble iNKT TCR to hCD1d molecules loaded with GSL containing an identical polar head can be fine tuned by modifying the length of the lipid chains.

It has recently been reported that diacylglycerol lipids from *Borrelia burgdorferi* are recognized by iNKT cells and that their antigenic potency is dependent on acyl chain length and saturation (3). In particular, it was shown that mouse iNKT cells more efficiently recognize mouse CD1d molecules loaded with diacylglycerol analogues with 16-carbon-long R_2 fatty acids. In contrast, human iNKT cells more efficiently recognize hCD1d molecules loaded with diacylglycerol analogues with 18-carbon-long R_2 fatty acids (3). It is likely that these differences between human and mouse iNKT cells can be accounted for by the shorter length of the mouse CD1d F′ channel as compared with the hCD1d F′ channel (4–7). However, these results did not address whether the enhanced potency of diacylglycerol analogues is caused by their more stable binding to CD1d molecules or rather to a higher TCR affinity. To distinguish between these possibilities, we independently analyzed the role of lipid chains occupying the A′ and F′ channels in hCD1d molecules in modulating the TCR affinity and/or stability of hCD1d–GSL complexes.

The central claim of this study is that the length of the lipid chain occupying the F′ channel modulates the binding affinity of iNKT TCR. This claim is supported by two complementary experimental systems: (a) SPR, analyzing the binding of soluble iNKT TCR to in vitro refolded CD1d molecules coated to BIAcore chips (Fig. 2, A and B), and (b) FACS staining, analyzing the binding of biotinylated tetramerized iNKT TCR to C1R-hCD1d cells pulsed with a panel of GSLs (Fig. 2 C).

The difference in TCR binding affinity between α-GalCer, OCH12, and OCH9 could be accounted for by the hypothesis that shortening of the phytosphingosine chain could cause a repositioning of this lipid chain in the hCD1d F′ channel and, thus, directly alter the position of the α-linked galactose or cause a shift in the α helices of hCD1d as a result of a collapse of the partially unfilled F′ channel.

If it is assumed that OCH9 retains the same orientation as α-GalCer, a comparison of the crystal structures of α-GalCer–loaded and empty hCD1d molecules (4) suggests that loading hCD1d molecules with OCH9 will only drive part of the F′ channel into the filled conformation because of the shorter phytosphingosine chain (Fig. 7 A). This modification results in predicted differences between hCD1d–OCH9 and hCD1d–α-GalCer structures of ∼2 Å in the main chain of the α2 helix between residues Leu139 and Thr154. This region is at the center of the putative TCR binding footprint as mapped by mutagenesis studies (22, 23) and includes two residues (Asp151 and Thr154) that hydrogen bond to the α-GalCer headgroup. Any substantial alterations in the positions of these residues may be expected to impact on the hydrogen bond network, which dictates the position of the headgroup, and, thus, to affect the recognition of α-GalCer by iNKT TCR.

These models and our finding that truncating the phytosphingosine chain decreases the k_{on} support a conformational change mechanism whereby hCD1d can exist in more than one conformation, a subset of which can bind iNKT TCR, and filling the F′ channel favors the TCR-binding conformations. A similar modeling exercise to assess the effect of shortening the acyl chain (i.e., the structural differences associated with incomplete occupation of the A′ channel; Fig. 7 B) predicts changes in the position of the α1 helix from residues Phe58 to Phe70, but, in contrast to the differences resulting from a partially unfilled F′ channel, these changes are in a region that is peripheral to the iNKT cell TCR docking area and have no influence on the orientation of the α-GalCer headgroup. Collectively, these structural considerations concur with our data, which indicate that changes in the length of the phytosphingosine but not the acyl chain can modulate TCR recognition.

The observation that fatty acid spacers have been identified in the A′ channel seems to suggest that the presence of these short-chain lipids could be a conserved element, ensuring full occupancy of the A′ channel (7, 21). In contrast, because the F′ channel can accommodate an alkyl chain up to

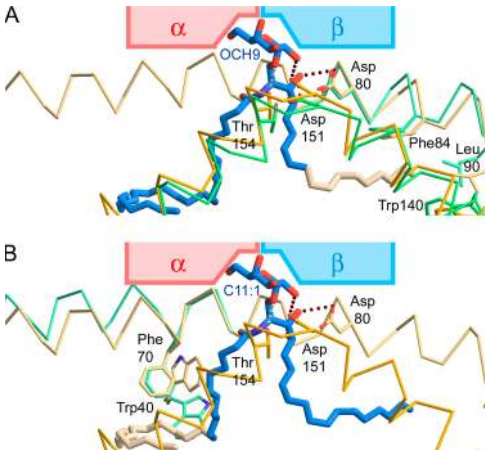

Figure 7. Modeling of the effects of variation in lipid chain length on the hCD1d structure. In both panels, a Cα trace and selected side chains are shown for the hCD1d crystal structure with bound α-GalCer (yellow), and relevant regions of the structure of hCD1d in the absence of bound ligand are shown in green. Hydrogen bonds are depicted as dotted lines. The putative position of bound TCR is indicated schematically. (A) The portion of α-GalCer in the crystal structure of hCD1d–α-GalCer, which corresponds to OCH9, is drawn in blue. Some side chains are positioned differently in the empty compared with α-GalCer–filled structure. Based on those differences, we have highlighted the residues that are predicted to move when OCH9 occupies the F′ channel as compared with their position in the α-GalCer–filled F′ channel. (B) The portion of α-GalCer that corresponds to a ligand with a shortened acyl chain (C11:1) is highlighted in blue. We have highlighted the side chains that are predicted to shift position based on a comparison of the empty and fully occupied (i.e., α-GalCer bound) hCD1d A′ channel.

18 carbon atoms long rather than 26 carbon atoms long, F′ channel spacer lipids are unlikely to exist when the F′ channel is occupied by lipid antigens shorter than 12 carbon atoms (such as OCH12 and OCH9) because fatty acids ranging from 9 to 6 carbon atoms required to fill the remaining unoccupied space of the F′ channel comprise only a minor percentage of the total fatty acid composition of mammalian cells (24).

We confirmed the results obtained using hCD1d molecules coated to the BIAcore chips by developing a FACS-based assay in which hCD1d molecules were expressed on live cells rather than coated to a solid phase (Fig. 2 C). The finding that fluorescently labeled recombinant iNKT TCR tetramers can be used as a staining reagent for GSL-pulsed C1R-CD1d cells is of interest because in a previous study, the staining of peptide-pulsed target cells by MHC class I–restricted TCR could only be obtained using an affinity-matured TCR with Kd values of $\sim 10^{-12}$ M (i.e., 10^6-fold higher than the affinity values of iNKT TCR; reference 25). Because iNKT TCR and wild-type MHC class I–restricted TCRs have similar affinities, it is tempting to speculate that the ability of iNKT TCR to stain GSL-pulsed cells may be caused by the clustering of hCD1d–GSL complexes on the surface of C1R-hCD1d cells.

Although the role of peptide MHC clustering in TCR signaling remains an area of investigation (26), a cooperative interaction between mouse CD1d–α-GalCer complexes and iNKT TCRs has previously been shown by fluorescence resonance energy transfer measurements (27). Our finding that the FACS-based assays confirmed the hierarchy of responses to the different GSLs observed in the SPR results strongly suggests that monomeric hCD1d/GSL–TCR interactions (i.e., SPR data) are in line with the situation in which the physiological multimeric hCD1d/GSL–TCR interactions may occur between hCD1d molecules expressed on the surface of APCs and TCRs expressed on iNKT cells. Consistent with our data, differences in the ability of mouse iNKT cells to be stained by mouse CD1d tetramers loaded with either α-GalCer or OCH9 have also been shown (27).

The use of a Fab antibody specific to the hCD1d–α-galactose–linked sphingolipid complex permitted us to compare the efficiency of binding to hCD1d molecules for a broad range of α-GalCer analogues. It is of interest that unlike iNKT TCR, Fab 9B has a more similar affinity for hCD1d monomers loaded with either α-GalCer or OCH9 (unpublished data), suggesting that the footprint of Fab 9B on the hCD1d–GSL complex may be different from the footprint of iNKT TCR. We used Fab 9B to study the role of each alkyl chain in controlling the rate of dissociation from hCD1d molecules. Consistent with previously published data with mouse CD1d molecules (28), we demonstrated that the shortening of either alkyl chain reduces the stability of the hCD1d–lipid complex. We further extended these results by demonstrating that the presence of two cis double bonds in the acyl chain, at positions 11 and 14 (C20:2; reference 6), reduced the rate of dissociation from hCD1d molecules as compared with the compound C20:0, which has a saturated acyl chain. It is of interest that the compound C20:2, unlike the compound C20:0, was shown to be efficiently loaded onto mouse CD1d molecules lacking an endosomal targeting motif, suggesting that the presence of the two double bonds at positions 11 and 14 could facilitate its binding to CD1d molecules (28). Because the acyl chain of α-GalCer is anchored in place in the A′ channel by circumnavigating a central pole (4), the observed differences in the rate of dissociation of the C20:0 and C20:2 compounds suggest that a preformed kink in the acyl chain caused by the presence of the unsaturated bonds may stabilize binding of the lipid by favoring the tightly curved conformation required for binding in the A′ channel.

Our results describe for the first time the immunological synapse of iNKT cells and polarization of iNKT cell cytotoxic granules. To determine the effect of the disparity in TCR affinities and TCR/hCD1d half-lives on the earliest events in human iNKT cell synapse formation, we used a planar lipid bilayer (15, 29) with constant ICAM-1 density and with equal numbers of hCD1d–OCH9 or hCD1d–α-GalCer complexes. The pattern of segregation of hCD1d molecules and ICAM-1 is similar to the pattern described for MHC class I– and II–restricted T cells (15). Interestingly, not only did the rate of accumulation of hCD1d–GSL complexes to cSMAC vary considerably between α-GalCer and OCH9, but the final density of aggregated antigen also differed.

The amount of signal that T cells receive by interacting with APCs is determined by several parameters, including the concentration of peptide MHC complex (class I peptide binding affinity) and the duration of the interaction between T cells and APCs (TCR binding affinity). Previous studies have compared the structures of peptide MHC complexes with those of altered peptide ligands, for example (30–35). Consistent with our findings describing the role of CD1d-bound lipid chains in modulating TCR binding affinity, these comparisons have demonstrated that substitutions of anchor residues can cause slight structural alterations that may indirectly impact on TCR recognition, synaptic strength, fluxing of calcium, and cytokine secretion (35–38).

T cell activation has recently been shown to be initiated and sustained in TCR-containing microclusters generated at the initial contact sites and at the periphery of the mature immunological synapse (39, 40). TCR signaling, which is sustained by stabilized microclusters, is terminated in the cSMAC, a structure from which TCRs are sorted for degradation (41). After the cSMAC forms, the microclusters continue to form and are sites of TCR signaling based on the recruitment of phosphorylated Lck, ZAP-70, and LAT (39, 40). Although analysis of microcluster formation in the immunological synapse of iNKT cells was beyond the scope of this study, our results indicate that the differential rate of accumulation of hCD1d–GSL complexes to the synapses substantially correlated with the strength of the subsequent iNKT cell stimulation.

When we compared hCD1d–α-GalCer with hCD1d–OCH9-stimulated synapses, hCD1d–α-GalCer–stimulated

synapses triggered a stronger and more rapid fluxing of calcium into the iNKT cells. Thus, the strength of signaling through the iNKT cell TCR is far greater for α-GalCer than for OCH9, and this determines downstream responses by the human iNKT cells. To strengthen these conclusions, we also compared the pattern of aggregation in lipid bilayers of hCD1d molecules loaded with OCH9 and C20:0 and demonstrated that the pattern and kinetics of hCD1d aggregation is very similar to those obtained with hCD1d–α-GalCer monomers. OCH9 and C20:0 have a similar rate of dissociation from hCD1d molecules, strongly suggesting that differences in the iNKT cell TCR affinity are controlling the pattern of hCD1d clustering in the lipid bilayers. Because the comparison of the binding kinetics of iNKT TCR to the hCD1d monomers loaded with different lengths of phytosphingosine chains was as much the result of decreases in the k_{on} as increases in the k_{off}, our results are consistent with previously published data, demonstrating that the differential accumulation of peptide MHC to cSMAC is ascribed to the TCR half-life for the peptide MHC complex (15). A recent study by Qi et al. (42) explores this concept further by providing an algorithm for relating solution half-life to 2D half-life by incorporating the heat capacity.

Differences in lymphokine profiles and in the proliferation of iNKT cells from PBL stimulated with α-GalCer and OCH9 can be accounted for by a combined effect of the higher affinity of α-GalCer to hCD1d molecules and higher affinity of the iNKT cell TCR for the hCD1d−α-GalCer complex. The reduced killing of DCs pulsed with OCH9 as compared with the killing of DCs pulsed with α-GalCer is consistent with the reduced polarization of cytotoxic granules in iNKT cells stimulated with weaker agonists. Because it has been shown that activation in vivo of iNKT cells can assist priming of antigen-specific immune responses (43, 44) reduced lysis of DCs pulsed with OCH9 suggests that more attention should be focused on the use of weaker iNKT cell agonists that, unlike α-GalCer, may ensure a longer life span of APCs. This is particularly important because α-GalCer–pulsed DCs have already been used in clinical trials (45).

In conclusion, our results highlight the effects of variation in the length of lipid chains of exogenously loaded lipids occupying the CD1d F′ channel in fine tuning the affinity of TCR of hCD1d-restricted lymphocytes. Although further experiments are required to extend these findings to the recognition of endogenous loaded lipids, our results demonstrate that the sensitivity of TCR recognition of hCD1d-restricted T lymphocytes can extend to detect differences in lipid chains buried in the F′ channel, resulting in altered TCR binding kinetics and different levels of activation signals.

MATERIALS AND METHODS

Reagents and cell lines. GSLs were synthesized by a previously described strategy (46), and their structures were confirmed by mass spectrometry. Glucocerebrosides (Gaucher's spleen) were purchased from Sigma-Aldrich. Human Vα24 iNKT cell lines were generated and maintained as previously described (47) in RPMI medium (Sigma-Aldrich).

Protein expression and purification. hCD1d and β_2M protein were refolded with GSL shown in Fig. 1 by oxidative refolding chromatography using a protocol that was previously described (48).

Preparation of soluble heterodimeric TCRs. The generation of soluble TCR heterodimers was based on the procedure described by Boulter et al. (49). In brief, the Vα24 and Vβ11 iNKT cell TCR sequences were amplified by PCR from the cDNA of an established iNKT cell clone. The α and β chains were individually cloned into pGMT7 bacterial expression vectors encoding the c-Jun and v-Fos fragments, respectively. TCR chains were expressed, refolded, and purified as previously described (49).

Soluble biotinylated TCR was made by inserting a 15–amino acid AviTag recognition peptide (Avidity) after the c-Jun fragment of the α chain. In brief, the α chain Jun fragment was amplified by PCR and subcloned into a pGMT7 vector encoding the AviTag peptide. This new α protein was expressed, refolded with the β chain, and purified as before. The TCR heterodimer was biotinylated with BirA enzyme before the final SD75 gel filtration (50). The biotinylated TCR heterodimers were tetramerized by mixing at a 4:1 molar ratio with Extravidin-PE (Sigma-Aldrich).

SPR. The affinity and kinetic properties of Vα24 NKT TCR binding to hCD1d–lipid complexes were measured with a spectrometer (model 3000; Biacore) as previously described (51). The purified biotinylated hCD1d–lipid complexes were immobilized onto streptavidin-coated CM5 sensor chips (Biacore) at a level of ∼1,000 response U. In all experiments, hCD1d–β-GalCer molecules were used as negative controls. Equilibrium binding was performed at a flow rate of 10 μl/min from the lowest TCR concentration. To exclude any effect of lipid dissociation, which would result in a gradual decrease in the level of immobilized CD1d–lipid during the course of the experiment, the affinity was determined with both increasing (from low to highest) and decreasing (from highest to lowest) concentrations of TCR. The affinity values obtained were not significantly different, indicating that lipid dissociation during the course of the experiments had a negligible effect on the affinity measurements. The data was plotted using Origin software (OriginLab), and Kd values were calculated using the standard hyperbolic model. Kinetics of the TCR–hCD1d/lipid interactions was measured at 50 μl/min. Equilibrium dissociation constants (Kd) and k_{on} and k_{off} were obtained by nonlinear curve fitting of the binding curves obtained after subtracting the response in the reference flow cells with equations derived from the simple 1:1 Langmuir binding model using the BIA evaluation program (version 3.02.2; Biacore). SPR was also used to estimate the dissociation rate of GSL from hCD1d molecules. 1,000 response U of hCD1d monomers loaded with either α-GalCer, OCH9, OCH12, OCH15, C20:0, C20:2, or C11:1 were immobilized on a streptavidin-coated sensor chip. As a negative control, hCD1d–β-GalCer biotinylated monomers were used. The amount of hCD1d–GSL remaining at a particular time was measured by injecting saturating amounts (30 μl at 500 nM) of Fab 9B antibody.

iNKT TCR tetramer staining. C1R-hCD1d cells were pulsed with 10 μM, 5 μM, 1 μM, 500 nM, and 100 nM of lipid for 16 h at 37°C and washed twice in RPMI. Cells were incubated with iNKT cell TCR tetramers at 37°C for 30 min and washed again twice with ice-cold PBS/1% FCS. Samples were analyzed on a flow cytometer (FACSCalibur; BD Biosciences), and the data were processed using CellQuest software (BD Biosciences).

Planar lipid bilayers. The GPI-linked ICAM-1 protein was purified from transfected L cells as previously described (52). In brief, the protein was solubilized in 1% Triton X-100 buffer and captured on an anti–ICAM-1 YN1/1.7 antibody-coupled Sepharose column (*N*-hydroxysuccinimide–activated HiTrap; 1 ml; GE Healthcare). The protein was labeled with AlexaFluor532 (Invitrogen) and eluted at low pH. The purified, labeled GPI-linked ICAM-1 was reconstituted into liposomes by detergent analysis with 0.4 mM egg phosphatidylcholine (Avanti Polar Lipids, Inc.). Planar lipid bilayers were formed in FCS2 closed chambers as previously described (15). AlexaFluor532-labeled GPI-linked ICAM-1 liposomes and biotinylated lipids

were mixed with 1,2-dioleocyl-phosphatidylcholine lipids (Avanti Polar Lipids, Inc.) at different ratios to obtain the required molecular densities. The chambers were blocked with PBS and 2% FCS. Monobiotinylated CD1d monomers were loaded on the bilayers using AlexaFluor633-streptavadin (Invitrogen) as a bridging with the biotin lipids. The iNKT cells were injected into the 37°C chambers in chamber buffer (PBS, 0.5% FCS, 2 mM Mg^{2+}, 0.5 mM Ca^{2+}, and 1 g/liter D-glucose). Confocal fluorescence and differential interference contrast images were simultaneously obtained at specified times, and iNKT cell contact with the planar bilayer was visualized by IRM. Images were acquired on an inverted microscope (Axiovert LSM 510-META; Carl Zeiss MicroImaging, Inc.) with a 63× oil immersion objective (Carl Zeiss MicroImaging, Inc.) and analyzed by LSM 510 software (Carl Zeiss MicroImaging, Inc.).

Ca^{2+} influx assays. Intracellular Ca^{2+} influx was measured by confocal microscopy with a fluorometric assay. Cells were labeled with fluo-4FF calcium indicator (1 μM in culture medium; Invitrogen) for 30 min at room temperature, washed, and injected into the FCS2 closed chamber in chamber buffer. The Ca^{2+} flux was monitored by the increase of fluorescence at ~520 nm with an open pinhole to acquire the total signal. The total mean fluorescence per cell was quantified as the intensity in the selected cell − intensity in the neighboring area at each time point. Data represent the mean of 20 cells.

Confocal microscopy. C1R-hCD1d target cells were pulsed with 1 μg/ml, 100 ng/ml, 10 ng/ml, 1 ng/ml, 100 pg/ml, 10 pg/ml, or 1 pg/ml of either α-GalCer or OCH9 lipid for 16 h at 37°C and washed twice in RPMI. NKT cells and C1R-hCD1d cells were washed in RPMI, and each cell pellet was resuspended to a final concentration of 10^6 cells/ml in RPMI. NKT cells and targets were mixed 1:1, left for 5 min in suspension, plated on glass multiwell slides, and incubated for 20 min at 37°C. Cells were fixed in 100% methanol precooled to −20°C, washed in PBS, and blocked in PBS/2% BSA (Sigma-Aldrich). The cells were stained, and the slides were mounted in PBS containing 90% glycerol and 2.5% 1,4-diazabicyclo[2.2.2]octane. Samples were examined using a laser-scanning microscope (Radiance 2000 MP; Bio-Rad Laboratories), and the conjugation rate and granule polarization were quantified using an epifluorescent microscope (Axioplan 2; Carl Zeiss MicroImaging, Inc.).

DC viability assay. Monocyte-derived DCs were differentiated as described previously (53). Immature DCs were collected at day 4, and 30,000 cells were plated in 96-well flat-bottom plates with equal numbers of iNKT cells and different concentrations of lipids. Cells were incubated for 24 h before FACS analysis on a flow cytometer (FACSCalibur; BD Biosciences) with CellQuest software (BD Biosciences).

ELISA. C1R-hCD1d cells were pulsed for 2 h with GSLs and diluted to 10^6cells/ml. 10^5 cell-pulsed targets were incubated at 37°C with 10^4 iNKT cells in a final volume of 200 μl. After 18 h, the supernatants were harvested, and the concentrations of IFN-γ and IL-4 were determined by ELISA according to the manufacturer's instructions (Mabtech).

iNKT cell expansion. PBMCs were isolated from healthy donors' buffy coats by density gradient centrifugation over Lymphoprep (Nycomed). Monocytes were positively selected using anti-CD14 mAb–coated magnetic beads (MACS; Miltenyi Biotec), and monocyte-depleted lymphocyte fractions (CD14 negative) were frozen until needed. Monocytes were cultured as previously described with 50 ng/ml GM-CSF (Novartis) and 1,000 U/ml IL-4 in six-well plates at 4×10^5 cells/ml (3 ml/well). After 5 d, maturation was induced using bacterial LPS (1 μg/ml LPS of *Salmonella abortus equi*; Sigma-Aldrich). Immature and mature monocyte-derived DCs were phenotypically analyzed for maturation markers. 2×10^5 monocyte-derived DCs were pulsed with GSL for 2 h in 24-well plates in 200 μl RPMI 1640. 2×10^6 autologous lymphocytes were added in 1.8 ml of medium (5% human serum). After 3 d, 25 IU/ml IL-2 was added to cultures. Thereafter, cultures were fed every 3–4 d with fresh medium containing 1,000 U/ml IL-2. iNKT cell frequencies were determined using APC CD1d tetramer and Vα24 antibody (Serotec).

Structural modeling. The structural effects of binding lipid chains of various lengths to hCD1d were assessed by comparison of the hCD1d–α-GalCer and empty hCD1d crystal structures (Protein Data Bank code 1ZT4). Structural superposition used the Structure Homology Program (54), and analysis was performed using the interactive graphics display program O (55).

Online supplemental material. Fig. S1 shows iNKT TCR and Fab 9B antibody binding to immobilized hCD1d–GSL monomers. hCD1d complexed with α-GalCer, OCH12, OCH9, and β-GalCer were loaded onto a streptavidin-coated CM5 sensor chip. Fig. S2 shows equivalent loading of the C1R-hCD1d cells with different GSLs. Video 1 shows the time-lapse reconstruction of the kinetics of hCD1d–α-GalCer aggregation (density = 200 molecules/μm^2). Online supplemental material is available at http://www.jem.org/cgi/content/full/jem.20062342/DC1.

This work was funded by Cancer Research UK grants C399/A2291 and C399/A3213, a UK Medical Research Council grant, and a European Community European Autoimmune Polyendocrine Syndrome Consortium grant to V. Cerundolo as well as Cancer Research UK grants C375/A3964 and C375/A5261 and a UK Medical Research Council grant to E.Y. Jones. P.A. van der Merwe acknowledges support from the UK Medical Research Council. G.S. Besra acknowledges support from James Bardrick in the form of a Personal Research Chair, is a former Lister Institute-Jenner Research Fellow, and is supported by the UK Medical Research Council and the Wellcome Trust.

The authors have no conflicting financial interests.

Submitted: 7 November 2006
Accepted: 28 March 2007

REFERENCES

1. Brigl, M., and M.B. Brenner. 2004. CD1: antigen presentation and T cell function. *Annu. Rev. Immunol.* 22:817–890.
2. Brutkiewicz, R.R. 2006. CD1d ligands: the good, the bad, and the ugly. *J. Immunol.* 177:769–775.
3. Kinjo, Y., E. Tupin, D. Wu, M. Fujio, R. Garcia-Navarro, M.R. Benhnia, D.M. Zajonc, G. Ben-Menachem, G.D. Ainge, G.F. Painter, et al. 2006. Natural killer T cells recognize diacylglycerol antigens from pathogenic bacteria. *Nat. Immunol.* 7:978–986.
4. Koch, M., V.S. Stronge, D. Shepherd, S.D. Gadola, B. Mathew, G. Ritter, A.R. Fersht, G.S. Besra, R.R. Schmidt, E.Y. Jones, and V. Cerundolo. 2005. The crystal structure of human CD1d with and without alpha-galactosylceramide. *Nat. Immunol.* 6:819–826.
5. Zeng, Z., A.R. Castano, B.W. Segelke, E.A. Stura, P.A. Peterson, and I.A. Wilson. 1997. Crystal structure of mouse CD1: an MHC-like fold with a large hydrophobic binding groove. *Science.* 277:339–345.
6. Zajonc, D.M., I. Maricic, D. Wu, R. Halder, K. Roy, C.H. Wong, V. Kumar, and I.A. Wilson. 2005. Structural basis for CD1d presentation of a sulfatide derived from myelin and its implications for autoimmunity. *J. Exp. Med.* 202:1517–1526.
7. Zajonc, D.M., C. Cantu III, J. Mattner, D. Zhou, P.B. Savage, A. Bendelac, I.A. Wilson, and L. Teyton. 2005. Structure and function of a potent agonist for the semi-invariant natural killer T cell receptor. *Nat. Immunol.* 6:810–818.
8. Giabbai, B., S. Sidobre, M. Crispin, Y. Sanchez-Ruiz, A. Bachi, M. Kronenberg, I. Wilson, and M. Degano. 2005. Crystal structure of mouse CD1d bound to the self ligand phosphatidylcholine: a molecular basis for NKT cell activation. *J. Immunol.* 175:977–984.
9. Zajonc, D., G. Ainge, G. Painter, W. Severn, and I. Wilson. 2006. Structural characterization of mycobacterial phosphatidylinositol mannoside binding to mouse CD1d. *J. Immunol.* 177:4577–4583.
10. Gadola, S.D., M. Koch, J. Marles-Wright, N.M. Lissin, D. Shepherd, G. Matulis, K. Harlos, P.M. Villiger, D.I. Stuart, B.K. Jakobsen, et al.

2006. Structure and binding kinetics of three different human CD1d-α-galactosylceramide-specific T cell receptors. *J. Exp. Med.* 203:699–710.
11. Kjer-Nielsen, L., N.A. Borg, D.G. Pellicci, T. Beddoe, L. Kostenko, C.S. Clements, N.A. Williamson, M.J. Smyth, G.S. Besra, H.H. Reid, et al. 2006. A structural basis for selection and cross-species reactivity of the semi-invariant NKT cell receptor in CD1d/glycolipid recognition. *J. Exp. Med.* 203:661–673.
12. Miyamoto, K., S. Miyake, and T. Yamamura. 2001. A synthetic glycolipid prevents autoimmune encephalomyelitis by inducing TH2 bias of natural killer T cells. *Nature.* 413:531–534.
13. Oki, S., A. Chiba, T. Yamamura, and S. Miyake. 2004. The clinical implication and molecular mechanism of preferential IL-4 production by modified glycolipid-stimulated NKT cells. *J. Clin. Invest.* 113:1631–1640.
14. Ramstedt, B., P. Leppimaki, M. Axberg, and J.P. Slotte. 1999. Analysis of natural and synthetic sphingomyelins using high-performance thin-layer chromatography. *Eur. J. Biochem.* 266:997–1002.
15. Grakoui, A., S.K. Bromley, C. Sumen, M.M. Davis, A.S. Shaw, P.M. Allen, and M.L. Dustin. 1999. The immunological synapse: a molecular machine controlling T cell activation. *Science.* 285:221–227.
16. Silk, J.D., I.F. Hermans, U. Gileadi, T.W. Chong, D. Shepherd, M. Salio, B. Mathew, R.R. Schmidt, S.J. Lunt, K.J. Williams, et al. 2004. Utilizing the adjuvant properties of CD1d-dependent NK T cells in T cell-mediated immunotherapy. *J. Clin. Invest.* 114:1800–1811.
17. Rauch, J., J. Gumperz, C. Robinson, M. Skold, C. Roy, D.C. Young, M. Lafleur, D.B. Moody, M.B. Brenner, C.E. Costello, and S.M. Behar. 2003. Structural features of the acyl chain determine self-phospholipid antigen recognition by a CD1d-restricted invariant NKT (iNKT) cell. *J. Biol. Chem.* 278:47508–47515.
18. Moody, D.B., V. Briken, T.Y. Cheng, C. Roura-Mir, M.R. Guy, D.H. Geho, M.L. Tykocinski, G.S. Besra, and S.A. Porcelli. 2002. Lipid length controls antigen entry into endosomal and nonendosomal pathways for CD1b presentation. *Nat. Immunol.* 3:435–442.
19. Brossay, L., O. Naidenko, N. Burdin, J. Matsuda, T. Sakai, and M. Kronenberg. 1998. Structural requirements for galactosylceramide recognition by CD1-restricted NK T cells. *J. Immunol.* 161:5124–5128.
20. Parekh, V.V., A.K. Singh, M.T. Wilson, D. Olivares-Villagomez, J.S. Bezbradica, H. Inazawa, H. Ehara, T. Sakai, I. Serizawa, L. Wu, et al. 2004. Quantitative and qualitative differences in the in vivo response of NKT cells to distinct alpha- and beta-anomeric glycolipids. *J. Immunol.* 173:3693–3706.
21. Wu, D., D.M. Zajonc, M. Fujio, B.A. Sullivan, Y. Kinjo, M. Kronenberg, I.A. Wilson, and C.H. Wong. 2006. Design of natural killer T cell activators: structure and function of a microbial glycosphingolipid bound to mouse CD1d. *Proc. Natl. Acad. Sci. USA.* 103:3972–3977.
22. Burdin, N., L. Brossay, M. Degano, H. Iijima, M. Gui, I.A. Wilson, and M. Kronenberg. 2000. Structural requirements for antigen presentation by mouse CD1. *Proc. Natl. Acad. Sci. USA.* 97:10156–10161.
23. Sidobre, S., O.V. Naidenko, B.C. Sim, N.R. Gascoigne, K.C. Garcia, and M. Kronenberg. 2002. The V alpha 14 NKT cell TCR exhibits high-affinity binding to a glycolipid/CD1d complex. *J. Immunol.* 169: 1340–1348.
24. Gennis, R.B. 1989. Biomembranes: Molecular Structure and Function. Springer-Verlag New York, Inc., New York. 533 pp.
25. Purbhoo, M.A., D.H. Sutton, J.E. Brewer, R.E. Mullings, M.E. Hill, T.M. Mahon, J. Karbach, E. Jager, B.J. Cameron, N. Lissin, et al. 2006. Quantifying and imaging NY-ESO-1/LAGE-1-derived epitopes on tumor cells using high affinity T cell receptors. *J. Immunol.* 176: 7308–7316.
26. Krogsgaard, M., J.B. Huppa, M.A. Purbhoo, and M.M. Davis. 2003. Linking molecular and cellular events in T-cell activation and synapse formation. *Semin. Immunol.* 15:307–315.
27. Stanic, A.K., R. Shashidharamurthy, J.S. Bezbradica, N. Matsuki, Y. Yoshimura, S. Miyake, E.Y. Choi, T.D. Schell, L. Van Kaer, S.S. Tevethia, et al. 2003. Another view of T cell antigen recognition: cooperative engagement of glycolipid antigens by Va14Ja18 natural T(iNKT) cell receptor. *J. Immunol.* 171:4539–4551.
28. Yu, K.O., J.S. Im, A. Molano, Y. Dutronc, P.A. Illarionov, C. Forestier, N. Fujiwara, I. Arias, S. Miyake, T. Yamamura, et al. 2005. Modulation of CD1d-restricted NKT cell responses by using N-acyl variants of alpha-galactosylceramides. *Proc. Natl. Acad. Sci. USA.* 102:3383–3388.
29. Carrasco, Y.R., S.J. Fleire, T. Cameron, M.L. Dustin, and F.D. Batista. 2004. LFA-1/ICAM-1 interaction lowers the threshold of B cell activation by facilitating B cell adhesion and synapse formation. *Immunity.* 20:589–599.
30. Reid, S.W., S. McAdam, K.J. Smith, P. Klenerman, C.A. O'Callaghan, K. Harlos, B.K. Jakobsen, A.J. McMichael, J.I. Bell, D.I. Stuart, and E.Y. Jones. 1996. Antagonist HIV-1 Gag peptides induce structural changes in HLA B8. *J. Exp. Med.* 184:2279–2286.
31. Ding, Y.H., B.M. Baker, D.N. Garboczi, W.E. Biddison, and D.C. Wiley. 1999. Four A6-TCR/peptide/HLA-A2 structures that generate very different T cell signals are nearly identical. *Immunity.* 11:45–56.
32. Degano, M., K.C. Garcia, V. Apostolopoulos, M.G. Rudolph, L. Teyton, and I.A. Wilson. 2000. A functional hot spot for antigen recognition in a superagonist TCR/MHC complex. *Immunity.* 12:251–261.
33. Sharma, A.K., J.J. Kuhns, S. Yan, R.H. Friedline, B. Long, R. Tisch, and E.J. Collins. 2001. Class I major histocompatibility complex anchor substitutions alter the conformation of T cell receptor contacts. *J. Biol. Chem.* 276:21443–21449.
34. Luz, J.G., M. Huang, K.C. Garcia, M.G. Rudolph, V. Apostolopoulos, L. Teyton, and I.A. Wilson. 2002. Structural comparison of allogeneic and syngeneic T cell receptor-peptide-major histocompatibility complex complexes: a buried alloreactive mutation subtly alters peptide presentation substantially increasing V_β interactions. *J. Exp. Med.* 195:1175–1186.
35. Chen, J.L., G. Stewart-Jones, G. Bossi, N.M. Lissin, L. Wooldridge, E.M. Choi, G. Held, P.R. Dunbar, R.M. Esnouf, M. Sami, et al. 2005. Structural and kinetic basis for heightened immunogenicity of T cell vaccines. *J. Exp. Med.* 201:1243–1255.
36. Ehrlich, L.I., P.J. Ebert, M.F. Krummel, A. Weiss, and M.M. Davis. 2002. Dynamics of p56lck translocation to the T cell immunological synapse following agonist and antagonist stimulation. *Immunity.* 17:809–822.
37. Yachi, P.P., J. Ampudia, N.R. Gascoigne, and T. Zal. 2005. Nonstimulatory peptides contribute to antigen-induced CD8-T cell receptor interaction at the immunological synapse. *Nat. Immunol.* 6: 785–792.
38. Yachi, P.P., J. Ampudia, T. Zal, and N.R. Gascoigne. 2006. Altered peptide ligands induce delayed CD8-T cell receptor interaction–a role for CD8 in distinguishing antigen quality. *Immunity.* 25:203–211.
39. Campi, G., R. Varma, and M.L. Dustin. 2005. Actin and agonist MHC-peptide complex-dependent T cell receptor microclusters as scaffolds for signaling. *J. Exp. Med.* 202:1031–1036.
40. Yokosuka, T., K. Sakata-Sogawa, W. Kobayashi, M. Hiroshima, A. Hashimoto-Tane, M. Tokunaga, M.L. Dustin, and T. Saito. 2005. Newly generated T cell receptor microclusters initiate and sustain T cell activation by recruitment of Zap70 and SLP-76. *Nat. Immunol.* 6:1253–1262.
41. Varma, R., G. Campi, T. Yokosuka, T. Saito, and M.L. Dustin. 2006. T cell receptor-proximal signals are sustained in peripheral microclusters and terminated in the central supramolecular activation cluster. *Immunity.* 25:117–127.
42. Qi, S., M. Krogsgaard, M.M. Davis, and A.K. Chakraborty. 2006. Molecular flexibility can influence the stimulatory ability of receptor-ligand interactions at cell-cell junctions. *Proc. Natl. Acad. Sci. USA.* 103:4416–4421.
43. Hermans, I.F., J.D. Silk, U. Gileadi, M. Salio, B. Mathew, G. Ritter, R. Schmidt, A.L. Harris, L. Old, and V. Cerundolo. 2003. NKT cells enhance CD4+ and CD8+ T cell responses to soluble antigen in vivo through direct interaction with dendritic cells. *J. Immunol.* 171:5140–5147.
44. Fujii, S., K. Shimizu, C. Smith, L. Bonifaz, and R.M. Steinman. 2003. Activation of natural killer T cells by α-galactosylceramide rapidly induces the full maturation of dendritic cells in vivo and thereby acts as an adjuvant for combined CD4 and CD8 T cell immunity to a coadministered protein. *J. Exp. Med.* 198:267–279.
45. Chang, D.H., K. Osman, J. Connolly, A. Kukreja, J. Krasovsky, M. Pack, A. Hutchinson, M. Geller, N. Liu, R. Annable, et al. 2005. Sustained expansion of NKT cells and antigen-specific T cells after injection of α-galactosyl-ceramide loaded mature dendritic cells in cancer patients. *J. Exp. Med.* 201:1503–1517.

46. Figueroa-Perez, S., and R.R. Schmidt. 2000. Total synthesis of alpha-galactosyl cerebroside. *Carbohydr. Res.* 328:95–102.
47. Gadola, S.D., N. Dulphy, M. Salio, and V. Cerundolo. 2002. Valpha24-JalphaQ-independent, CD1d-restricted recognition of alpha-galactosylceramide by human CD4(+) and CD8alphabeta(+) T lymphocytes. *J. Immunol.* 168:5514–5520.
48. Karadimitris, A., S. Gadola, M. Altamirano, D. Brown, A. Woolfson, P. Klenerman, J.L. Chen, Y. Koezuka, I.A. Roberts, D.A. Price, et al. 2001. Human CD1d-glycolipid tetramers generated by in vitro oxidative refolding chromatography. *Proc. Natl. Acad. Sci. USA.* 98:3294–3298.
49. Boulter, J.M., M. Glick, P.T. Todorov, E. Baston, M. Sami, P. Rizkallah, and B.K. Jakobsen. 2003. Stable, soluble T-cell receptor molecules for crystallization and therapeutics. *Protein Eng.* 16:707–711.
50. O'Callaghan, C.A., M.F. Byford, J.R. Wyer, B.E. Willcox, B.K. Jakobsen, A.J. McMichael, and J.I. Bell. 1999. BirA enzyme: production and application in the study of membrane receptor-ligand interactions by site-specific biotinylation. *Anal. Biochem.* 266:9–15.
51. Willcox, B.E., G.F. Gao, J.R. Wyer, J.E. Ladbury, J.I. Bell, B.K. Jakobsen, and P.A. van der Merwe. 1999. TCR binding to peptide-MHC stabilizes a flexible recognition interface. *Immunity.* 10:357–365.
52. Bromley, S.K., A. Iaboni, S.J. Davis, A. Whitty, J.M. Green, A.S. Shaw, A. Weiss, and M.L. Dustin. 2001. The immunological synapse and CD28-CD80 interactions. *Nat. Immunol.* 2:1159–1166.
53. Salio, M., D. Shepherd, P.R. Dunbar, M. Palmowski, K. Murphy, L. Wu, and V. Cerundolo. 2001. Mature dendritic cells prime functionally superior melan-A-specific CD8+ lymphocytes as compared with nonprofessional APC. *J. Immunol.* 167:1188–1197.
54. Stuart, D.I., M. Levine, H. Muirhead, and D.K. Stammers. 1979. Crystal structure of cat muscle pyruvate kinase at a resolution of 2.6 A. *J. Mol. Biol.* 134:109–142.
55. Jones, T.A., J.Y. Zou, S.W. Cowan, and M. Kjeldgaard. 1991. Improved methods for building protein models in electron density maps and the location of errors in these models. *Acta. Crystallogr. A.* 47:110–119.